Received: 3 October 2023 | Revised: 10 November 2023 | Accepted: 20 November 2023

DOI: 10.1002/dad2.12515

Alzheimer's & Dementia
Diagnosis, Assessment & Disease Monitoring

RESEARCH ARTICLE

Combined 18F-FDG PET-CT markers in dementia with Lewy bodies

Maria Vittoria Mattoli[1,2] | **Fabrizio Cocciolillo**[3] | **Piero Chiacchiaretta**[4,5] | **Francesco Dotta**[4] | **Gianluca Trevisi**[1] | **Claudia Carrarini**[6,7] | **Astrid Thomas**[1] | **Stefano Sensi**[1] | **Andrea Delli Pizzi**[4] | **Angelo Domenico Di Nicola**[2] | **Adolfo Di Crosta**[8,9] | **Nicola Mammarella**[8] | **Alessandro Padovani**[10] | **Andrea Pilotto**[10,11] | **Fabio Moda**[12] | **Pietro Tiraboschi**[12] | **Gianluigi Martino**[13] | **Laura Bonanni**[9]

[1]Department of Neuroscience, Imaging and Clinical Sciences, University G. d'Annunzio of Chieti-Pescara, Chieti, Italy

[2]Nuclear Medicine Unit, Presidio Ospedaliero Santo Spirito, Pescara, Italy

[3]Dipartimento di Diagnostica per Immagini, Radioterapia Oncologica ed Ematologia, UOC di Medicina Nucleare, Fondazione Policlinico Universitario Agostino Gemelli IRCCS, Rome, Italy

[4]Department of Innovative Technologies in Medicine and Dentistry, University G. d'Annunzio of Chieti – Pescara, Chieti, Italy

[5]Advanced Computing Core, Center for Advanced Studies and Technology - C.A.S.T, University G. d'Annunzio of Chieti – Pescara, Chieti, Italy

[6]Department of Neuroscience, Catholic University of Sacred Heart, Rome, Italy

[7]IRCCS San Raffaele, Rome, Italy

[8]Department of Psychological Science, Humanities and Territory, University "G. d'Annunzio" of Chieti-Pescara, Chieti, Italy

[9]Department of Medicine and Aging Sciences, University G d'Annunzio of Chieti-Pescara, Chieti, Italy

[10]Neurology Unit, Department of Clinical and Experimental Sciences, University of Brescia, Brescia, Italy

[11]Parkinson's Disease Rehabilitation Centre, FERB ONLUS-S. Isidoro Hospital, Trescore Balneario, Bergamo, Italy

[12]Division of Neurology 5 and Neuropathology, Fondazione IRCCS Istituto Neurologico Carlo Besta, Milan, Italy

[13]Department of Radiological Sciences, Nuclear Medicine Unite, SS. Annunziata Hospital, Via dei Vestini 31, Chieti, Italy

Correspondence
Laura Bonanni, Department of Medicine and Aging Sciences, University G d'Annunzio of Chieti-Pescara Via dei Vestini 31, 66100 Chieti, Italy.
Email: l.bonanni@unich.it

Funding information
Italian Ministry of Health, Grant/Award Number: RF-2018-12366209

Abstract

INTRODUCTION: ^{18}F-Fluoro-deoxyglucose–positron emission tomography (FDG-PET) is a supportive biomarker in dementia with Lewy bodies (DLB) diagnosis and its advanced analysis methods, including radiomics and machine learning (ML), were developed recently. The aim of this study was to evaluate the FDG-PET diagnostic performance in predicting a DLB versus Alzheimer's disease (AD) diagnosis.

METHODS: FDG-PET scans were visually and semi-quantitatively analyzed in 61 patients. Radiomics and ML analyses were performed, building five ML models: (1) clinical features; (2) visual and semi-quantitative PET features; (3) radiomic features; (4) all PET features; and (5) overall features.

RESULTS: At follow-up, 34 patients had DLB and 27 had AD. At visual analysis, DLB PET signs were significantly more frequent in DLB, having the highest diagnostic accuracy (86.9%). At semi-quantitative analysis, the right precuneus, superior parietal, lateral occipital, and primary visual cortices showed significantly reduced uptake in DLB. The ML model 2 had the highest diagnostic accuracy (84.3%).

DISCUSSION: FDG-PET is a valuable tool in DLB diagnosis, having visual and semi-quantitative analyses with the highest diagnostic accuracy at ML analyses.

KEYWORDS

18F-FDG, artificial intelligence, biomarkers, dementia, Lewy body dementia, machine learning, PET-CT, radiomics

1 | BACKGROUND

Dementia with Lewy bodies (DLB) is a common neurodegenerative condition in the elderly,[1] representing 15%–20% of dementia cases in post-mortem examination.[2,3]

The pathologic hallmark of DLB consists of Lewy-related pathology (LRP), characterized by abnormal accumulation and aggregation of α-synuclein in neurons.[4,5] Currently, no direct in vivo biomarker for LRP is available.

Diagnosis of DLB is based on consensus criteria,[6] but the accuracy of the clinical diagnosis of DLB is not satisfactory, with many cases missed or misdiagnosed. Indeed, the clinical presentation may overlap with other forms of neurodegenerative dementia, especially Alzheimer's disease (AD).[7]

Moreover, in a high percentage of patients with dementia, multiple neurodegenerative pathologies coexist.[6,8] Indeed, DLB and AD can often be associated: almost 90% of patients with DLB have moderate to abundant cortical amyloid plaques.[9] Thus, in these patients with mixed pathologies, the clinical diagnosis is even more difficult.

The use of biomarkers, including nuclear medicine functional imaging, can contribute to enhance diagnostic accuracy.[10,11]

In particular, positron emission tomography (PET) technique with ^{18}F-Fluoro-deoxyglucose (^{18}F-FDG) can detect the following markers of DLB: (1) a reduction of glucose metabolism in the occipital cortex, along with a bilateral parietotemporal hypometabolism[12–15]; and (2)a relative preservation of glucose metabolism at of the posterior cingulate cortex compared to the cuneus and precuneus,[16] the so-called cingulate island sign (CIS). These two indices are considered supportive biomarkers for DLB.[6]

Recently, an occipital tunnel sign (OTS) was described,[17] which results from relative sparing of ^{18}F-FDG uptake in the mesial occipital (primary visual) cortex compared with more severe loss in the surrounding lateral occipital (visual association) cortex, especially in sagittal projections. More recently, a relative preservation of metabolism in the amygdala on PET with ^{18}F-FDG (FDG-PET) as a potential imaging marker for DLB, named the amygdala sign (AS), has also been reported.[18]

The analysis of nuclear medicine biomarkers in DLB can be performed by visual assessment of images, which depends highly on the observer's experience with possible variance in reduced sensitivity and specificity of the marker among centers; by automatic semi-quantitative methods, including three-dimensional stereotactic surface projections (3D-SSP), which is based on statistical mapping method,[19,20] where the pixel values on FDG-PET images are normalized to the value of a reference region (pons or cerebellum).[21,22] An image set from a single subject is then compared to a database obtained from multiple normal subjects, which is embedded within the system and can be further implemented according to the needs of the center and expressed as a *Z*-score.[20,23]

In recent years, radiomics and artificial intelligence (AI) methods, including machine learning (ML) in medical image analysis, have been applied successfully to neurological diseases, including dementia and parkinsonism.[24,25] Radiomics analysis is an advanced technique focused on extracting a wide range of quantitative features, including texture, shape, and intensity parameters, from nuclear medicine images, including FDG-PET.[26] The extracted radiomic features are then utilized in combination with ML algorithms, which analyze the radiomic features to identify correlations, relationships, or meaningful patterns. Leveraging radiomics and ML analysis, more detailed information can be obtained, revealing subtle or complex aspects of the PET/computed tomography (PET-CT) images that may not be immediately apparent during qualitative or semi-quantitative analysis.[27]

The aim of our study was to evaluate the diagnostic performance of combined nuclear medicine indices of DLB (i.e., occipital hypometabolism, CIS, OTS, and AS), integrated with clinical information, and analyzed with different methods, including visual, semi-quantitative, radiomics, and ML with automatic classification in predicting the final clinical diagnosis of DLB versus AD.

2 | METHODS

2.1 | Study population

From November 2018 to February 2022, a total of 96 consecutive patients (median age 72.3, range 55–92; 42 female) referred to the University of Chieti-Pescara Neurological Department for cognitive

impairment (Montreal Cognitive Assessment [MoCA]; mean ± SD: 18.76 ± 5.2) underwent brain PET-CT with FDG-PET scan.

From this large clinical cohort, we retrospectively selected patients according to the following inclusion criteria: (1) brain FDG-PET for functional assessment; (2) clinical diagnosis of probable DLB according to revised diagnostic criteria,[6] and for comparison, probable AD based on the National Institute on Aging and the Alzheimer's Association (NIA-AA) and the European Federation of Neurological Societies/European Neurological Society (ENS-EFNS) criteria[28]; (3) minimum duration of neurological and neuropsychological follow-up of 12 months after the first clinical evaluation.

All selected patients were evaluated for neurological and internal diseases (i.e., hypertension and diabetes mellitus). Laboratory analyses excluded secondary cognitive disorders, and patients with ascertained neurological diseases other than DLB and psychiatric diseases were excluded.

All selected patients underwent neurological examination, neuropsychological tests (MoCA) and magnetic resonance imaging (MRI), for morphological brain assessment and to exclude the presence of brain tumors or of major cortical atrophy.

The standard of reference was final diagnosis of DLB/AD, defined retrospectively by a multidisciplinary team (MDT) including experienced dementia specialists, neuropsychologists, radiologists, and nuclear medicine physicians of University of Chieti-Pescara, after a clinical follow-up of a minimum of 12 months after the first neurological evaluation. The final clinical diagnosis was also based on the biomarkers available for each patient.

Before the FDG-PET procedure, written informed consent was obtained from all patients, and their data were treated in accordance with the local privacy rules and regulations. In the informed consent, the patients signed to accept that their data could be used for scientific purposes. This study was approved by the local Chieti-Pescara Ethic Committee (approval number 13, 06/27/2019). The present study was in accordance with the ethical standards as laid down in the 1964 Declaration of Helsinki and its later amendments or comparable ethical standards.

2.2 | Acquisition protocol of brain FDG PET-CT

Patients underwent an FDG brain scan using a PET-CT Discovery MI DR scanner (GE Healthcare; 3.27 mm thickness; 5.55 mm in-plane full-width half maximum [FWHM]). The FDG-PET acquisition procedures were conformed to the European Association of Nuclear Medicine guidelines.[29]

The patient, fasted for at least 6 hours, was positioned supine in a quiet and soft light condition for about 15 minutes before FDG administration. Blood glucose level was checked prior to administration, and it was <160 mg/dL (<8.9 nmol/L) in all patients. The scan was obtained over 15 minutes, starting 45 minutes after intravenous injection of 125–250 MBq (typically 185 MBq). All images were reconstructed using an ordered subset-expectation maximization (OSEM) algorithm, and the CT scan (120 kV) was used for attenuation correction. Each reconstructed image was inspected visually to check for major artifacts.

The images were visually and semi-quantitatively analyzed. In addition, radiomics and ML techniques were applied to perform a more detailed analysis of the images.

RESEARCH IN CONTEXT

1. **Systematic review**: to date, ^{18}F-Fluoro-deoxyglucose–positron emission tomography (FDG-PET) is a supportive biomarker for dementia with Lewy bodies (DLB) diagnosis, and different PET signs have been described. Advanced FDG-PET analysis methods, including radiomics and machine learning, were recently developed.
2. **Interpretation**: Our findings support the high diagnostic performance of FDG-PET in predicting DLB versus Alzheimer's disease (AD) by using both visual and semi-quantitative analyses. Our results showed that DLB PET signs were significantly more frequent in DLB at visual PET analysis (accuracy of 86.9%), whereas, at semi-quantitative analysis, right precuneus, superior parietal, lateral occipital, and primary visual cortices showed significantly reduced uptake in DLB.
3. **Future directions**: FDG-PET is a valuable and helpful tool for differentiating DLB from other clinical entities, such as AD. FDG-PET reading techniques as visual and semi-quantitative analyses show the highest diagnostic accuracy.

2.3 | Visual analysis of FDG PET-CT images

^{18}FDG PET-CT brain transverse, sagittal, and coronal images were assessed separately by two nuclear medicine physicians with more than 15 years of experience in PET and Single photon emission computer tomography (SPECT) neuroimaging (M.V.M. and F.C.). The two specialists were informed about the potentially pathological conditions of the patients but blinded to the neurological evaluations. The GE scale was used to normalize the images with a uniform uptake threshold, using the basal ganglia and the cerebellum as a reference to background regions.

Data interpretation took into consideration global changes and regional decreases in FDG uptake. The images were classified as normal, indicative for DLB or indicative for AD, according to the most typical hypometabolic pattern in neurodegenerative diseases.[23] Particularly, an exam was considered as normal in the case of homogenous and symmetric tracer uptake in cortical areas of both hemispheres. Patients whose cortical areas showed reduced glucose metabolism in the regions including the lateral/medial occipital cortex, temporoparietal cortex, and frontal cortex, along with a relative preservation

of the mid/posterior cingulate region, were classified as DLB-like metabolic pattern. In addition, we noted the presence of a series of features or signs described as in association with DLB, namely: (1) the presence/absence of hypometabolism in the occipital lobes[6]; (2) the presence of CIS, consisting of the sparing of the posterior cingulate relative to the precuneus and cuneus[30]; (3) the presence of OTS, resulting from sparing of medial occipital lobe (primary visual cortex) relative to the lateral occipital lobe (associative visual cortex) in sagittal projections[17]; and (4) the presence of AS, consisting of the relative preservation of amygdala metabolism.[18] Patients with hypometabolism in the posterior cingulate, the precuneus, the parietal cortical territories, and the medial and lateral temporal cortex were classified as AD-like metabolic pattern.

2.4 | Semi-quantitative analysis of FDG PET-CT images

The FDG-PET images were semi-quantitatively analyzed at the individual level. Semi-quantitative analysis was performed on a commercially available fully-automated post-processing software (Cortex ID SUITE, GE Healthcare, Chicago, IL, USA).[24,31] All scans, spatially realigned and normalized, were sampled at 16,000 predefined cortical locations. Individual maps of hypometabolism were generated using 3D-SSP, providing stereotactic surface projection displays.[32] Standardized uptake values were obtained for 25 regions of interest (ROIs) and normalized to the pons. The regions were prefrontal lateral left (L) and right (R), prefrontal medial L and R, sensorimotor L and R, anterior cingulate L and R, posterior cingulate L and R, precuneus L and R, parietal superior L and R, parietal inferior L and R, occipital lateral L and R, primary visual L and R, temporal lateral L and R, temporal mesial L and R, and whole cerebellum. Individual patient's ROI Z-scores were calculated from 294 healthy sex- and age-matched controls,[33] with a Z-score ← 2.0 as cut-off for significant hypometabolism (Z-score = [mean database-mean subject]/SD database).

Furthermore, the DLB hallmark signs were semi-quantitatively calculated on PET count-rate data according to the following ROI-based methods: (1) CIS ratio, consisting of the ratio of the median value of counts in the posterior cingulate to cuneus plus precuneus; (2) OTS ratio, consisting of the ratio of the median value of counts in the medial occipital cortex to the lateral occipital cortex; and (3) AS ratio (right and left) consisting of the ratio of the median value of counts in the medial temporal cortex to the lateral temporal cortex.

2.5 | Radiomic features and machine-learning analysis: Image pre-processing and volume of interest selection

All reconstructed volumes were analyzed using Statistical Parametric Mapping 8 (SPM, Wellcome Department of Cognitive Neurology, University College London, UK). To place images in the standard Montreal Neurological Institute neuroanatomic space (MNI; http://www.bic.mni.mcgill.ca), an FDG template was used as reference. The SPM8 normalization algorithm was employed to register FDG-PET images with the template, using the following setting: a 12-parameter affine transformation, a nonlinear frequency cutoff of 25 mm, and 16 nonlinear iterations and a nonlinear regularization switched at 1. A trilinear interpolation was applied during the final re-slicing. Each scan was visually checked after spatial normalization for shape artifacts. The dimensions of output volumes were the following: $x = -90{:}91$, $y = -126{:}91$, and $z = -72{:}109$ from the anterior commissure, with a $2 \times 2 \times 2$ mm^3 isotropic voxel. Spatially normalized images were subsequently intensity normalized to correct for differences in total brain counts between scans using global mean scaling method by scaling the images to the average FDG uptake value in the whole brain. Volume of interests (VOIs) for all normalized images were selected from the digital atlas resulting from an automatic anatomic segmentation of the spatially normalized, single subject, high-resolution T1 MRI data set provided by the MNI (Automated Anatomical Labeling—AAL of Activations in SPM),[34] for a total of 116 labels through the brain. In order to better compare the results between the ML analysis and the semi-quantitative analysis with CortexID (consisting in 25 ROIs), we summed contiguous SPM-VOIs to obtain larger areas overlapping with CortexID-derived ROIs, resulting in a final number of 39 VOIs: basal ganglia left (L) and right (R), calcarine L and R, central region L and R, cerebellum L and R, anterior cingulate L and R, posterior cingulate L and R, frontobasal L and R, fusiform L and R, insula L and R, occipital lateral L and R, occipital mesial L and R, parietal inferior L and R, parietal superior L and R, precuneus L and R, prefrontal lateral L and R, prefrontal medial L and R, temporal lateral L and R, temporal mesial L and R, thalamus L and R, and vermis. Each selected VOI included up to nine brain areas labeled (see Table S1).

The following parameters were calculated (1) Variance, calculated as the average of the squared distances of each intensity value from the mean value. Variance measures the spread of the intensity distribution relative to the mean. Thus the variance represents how much the intensity within the mask varies compared to the intensities in other brain regions. (2) Skewness, which measures the asymmetry of the value distribution with respect to the mean value. Depending on the concentration of this distribution, its value can be positive or negative. (3) Energy, a measure of the magnitude of voxel values in an image. It sums the squares of these values to obtain the final measure for the entire mask. (4) Kurtosis, a measure of the "peakedness" of the value distribution within the image's ROI. For instance, a higher kurtosis value indicates that the values are concentrated primarily toward the tails rather than the mean, whereas a lower kurtosis value indicates a concentration of values around the mean.

2.6 | Extraction of radiomics features and machine learning analysis

The machine learning analysis was developed in Python 3.9, using PyRadiomics for feature extraction[35] and the combination of Boruta,[36]

as the feature selection algorithm, and Random forest, as the classifier of the model.[37]

PyRadiomics is an open-source package for the extraction of radiomics features from medical imaging with the goal of establishing a reference standard for radiomic analysis.[35] The feature selection methods developed in this study have selected only PyRadiomics' "first-order features," which are obtained by describing the distribution of voxel intensities within the image region defined by the mask through commonly used and basic metrics (https://pyradiomics.readthedocs.io/en/latest). A total of five ML models were implemented using different combinations of FDG-PET and clinical features: (1) clinical features, consisting of age, sex, education, MoCA, and symptoms (i.e., visual hallucinations, cognitive fluctuations, rapid eye movement (REM) sleep behavior disorder (RBD), parkinsonism, delirium, psychiatric symptoms, language changes); (2) standard PET features, consisting of DLB hallmark signs (either visually or semi-quantitatively assessed) along with the *Z*-score values of each brain region extracted by Cortex ID; (3) radiomics features, extracted by PyRadiomics from FDG-PET images; (4) all PET features, consisting of the combination of standard PET features (see above) and radiomics features; and (5) overall features, consisting of the combination of all the data available, that is, all PET features (see above) and clinical features.

All five machine learning models were developed following a consistent workflow: (1) The data set was partitioned randomly into a training set, which accounted for 70% of the data, and a testing set, comprising the remaining 30%, to minimize selection bias; (2) dimensionality reduction was achieved using the Boruta algorithm to identify relevant features for the analyses; and (3) classification tasks were conducted employing the random Forest classifier, which was trained on the training set. The model's performance was evaluated subsequently on the testing set using traditional statistical metrics, including accuracy, specificity, sensitivity, precision for DLB, and precision for AD.

2.7 | Statistical analysis

Final diagnosis from MDT consensus was used to divide patients into two groups: AD group and DLB group. Main demographic, clinical, and PET-derived data were compared between the two groups. Descriptive statistics was used to describe main demographic, clinical, and PET-derived data for all patients. The same variables were compared between the two MDT-derived diagnosis groups (AD and DLB). Quantitative variables are presented as the mean ± SD, and the Student's *t*-test was used for comparison. If the equal variance assumption was violated, a Welch test was used instead of the Student's *t*-test. The chi-square test or, when more appropriate, the Fisher exact test (two-sided), was used to compare the categorical variables.

When comparing differences between the AD and DLB groups regarding semi-quantitative results derived from FDG-PET, namely, *Z*-scores of different cerebral areas derived from the 3D-SSP, we first examined all populations; then we excluded those PET exams considered negative at nuclear medicine physicians' examination.

For those cerebral areas that showed a significant difference of *Z*-scores between the AD and DLB groups, we built receiver-operating characteristic (ROC) and calculated the area under the curve (AUC) to score their performance to classify patients between the two pathologies and to identify the optimal *Z*-score cutoff value. Again, first, we analyzed the entire cohort, including negative PETs, and then we performed a subgroup analysis of positive PETs only.

Afterward, we analyzed FDG-PET diagnostic accuracy using MDT final diagnosis as a gold standard reference. First, we assessed PET diagnostic accuracy metrics for both AD and DLB in the entire population cohort. Namely, we diagnosed patients as affected by DLB or, in a second analysis, by AD, based on PET. Therefore, negative PETs were included in this analysis and evidently counted as negative exams (either false negatives or true negatives). Finally, we excluded negative PETs and measured diagnostic accuracy metrics for those cases where PET had a pathological appearance and could contribute to the final diagnosis.

The following metrics were assessed: sensitivity, specificity, accuracy, positive predictive value (PPV), and negative predictive value (NPV). Jamovi version 2.3.24 open R-based software was used for statistical analysis. *P*-values < 0.05 were considered statistically significant.

3 | RESULTS

3.1 | Population

Sixty-one patients met the inclusion criteria (mean age 74.9 ± 7.81 years, range 57-92; 24 female; education 9.34 ± 4 years, range 1–18). Median follow-up from the FDG-PET to the final clinical evaluation was 16.8 ± 6.2 months.

According to the final clinical diagnosis (MDT), 34 of 61 (55.7%) and 27 of 61 (44.3%) of patients had a final clinical diagnosis of DLB and AD, respectively. No significant difference was found in the demographic, education, and cognitive characteristics between the two patient groups, as shown in Table 1.

TABLE 1 Demographic, education, and clinical features in all patients according to final clinical diagnosis (MDT).

	DLB	AD	*p*
Participants (*n*)	34	27	
Age (years)	76.56 (8.09)	72.89 (7.07)	0.07
Sex (M/F)	21/13	16/11	0.8
Education (years)	8.76 (3.7)	10.07 (4.3)	0.2
MoCA	20.09 (5.54)	19.43 (4.49)	0.62
Visual hallucinations	14 (41.2%)	2 (7.4%)	0.003
Cognitive fluctuations	28 (82.3%)	10 (37%)	<0.001
RBD	21 (61.8%)	1 (3.7%)	<0.001
Parkinsonism	22 (64.7%)	8 (29.6%)	0.006
Delirium	8 (23.5%)	3 (11.1%)	0.2
Psychiatric symptoms	17 (50.0%)	11 (40.7%)	0.5

Note: Data are shown as number (%) or mean (SD).

DLB final diagnosis was supported by electroencephalography (EEG; dominant pre-alpha rhythm with high dominant frequency variability[10]) and by Dopamine transporter (DAT)-SPECT with 123I-FP-CIT for dopaminergic evaluation, which was performed in 25 of 34 (73.5%) DLB patients, all of them showing a reduction of striatum uptake.[38] All patients with an AD final diagnosis were ^{18}F-flutemeltamol PET-CT positive for cerebral amyloid deposition. Furthermore, 5 of 26 patients with a final clinical diagnosis of AD underwent 123I-FP-CIT, all with negative result; 10 of 34 patients with a final clinical diagnosis of DLB had an 18F-flutemeltamol PET-CT scan, all with a negative result. MoCA: Montreal cognitive assessement; RBD: REM sleep behaviour disorder.

When comparing final clinical diagnosis (MDT) with the presence of clinical features in all patients (i.e., visual hallucinations, cognitive fluctuations, RBD, parkinsonism, delirium, psychiatric symptoms, Table 1), patients with a final clinical diagnosis of DLB had more frequent visual hallucinations ($p = 0.003$), cognitive fluctuations ($p < 0.001$), RBD ($p < 0.001$), and parkinsonism ($p = 0.006$) compared with patients with AD.

3.2 | Visual analysis of FDG PET-CT images

According to visual evaluation, FDG-PET was considered positive in 54 of 61 patients (88.5%) and negative in 7 of 61 patients (11.4%).

Among the 54 patients with positive FDG-PET scans, a DLB-like metabolic pattern was identified in 26 (48.15%), whereas the readers identified the AD-like metabolic pattern in 28 patients (51.85%).

Two patients with AD-like metabolic patterns were eventually diagnosed as DLB at MDT consensus. No one with a DLB-like metabolic pattern was finally diagnosed as AD at MDT consensus. Regarding the negative FDG-PET scans ($n = 7$), six PET-negative patients were diagnosed as DLB and one PET-negative patient as AD, according to the final clinical diagnosis (MDT).

Therefore, the overall concordance between the FDG-PET hypometabolic pattern (DLB-like and AD-like) and the final clinical diagnosis (MDT) was 26 of 34 (76.5%) for DLB and 26 of 27 (96.3%) for AD patients. At visual analysis, patients with a final clinical diagnosis of DLB showed the presence of occipital hypometabolism, CIS, OTS, and AS more frequently than the group of AD patients ($p < 0.001$), as shown in Table 2.

The sensitivity, specificity, diagnostic accuracy, PPV, and NPV of the hypometabolic pattern at FDG-PET, and the DLB hallmark signs, that is, occipital hypometabolism, CIS, OTS, and AS, according to final clinical diagnosis (MDT) were shown in Table 3.

3.3 | Semi-quantitative analysis of FDG PET-CT images

Considering all patients ($n = 61$), univariate analysis returned only one area where the *Z*-score was significantly different between AD and DLB, such as the left mesial temporal cortex ($p = 0.027$), with a lower *Z*-score in AD patients.

Once excluding the seven patients with negative FDG-PET, and considering only the positive FDG-PET scans ($n = 54$), univariate analysis returned seven areas with significantly lower *Z*-scores in DLB compared with AD (Table 4), including the precuneus R ($p = 0.006$), parietal superior R ($p = 0.025$), parietal superior L ($p = 0.045$), occipital lateral R ($p = < 0.001$), occipital lateral L ($p = 0.027$), primary visual R ($p = 0.001$), and Primary visual L ($p = 0.017$).

As shown in Figure 1 and Table 4, ROC curve analysis confirmed a good accuracy for each of the above areas.

TABLE 2 Visually assessed DLB hallmark signs, that is, occipital hypometabolism, cingulate island sign, occipital tunnel sign, and amygdala sign, in the two patients' groups according to final clinical diagnosis (MDT).

	DLB	AD	*p*
Participants (*n*)	34	27	
Occipital hypometabolism	27 (79.4%)	6 (22.2%)	<0.001
CIS	22 (64.7%)	1 (3.7%)	<0.001
OTS	22 (64.7%)	1 (3.7%)	<0.001
AS	20 (58.8%)	3 (11.1%)	<0.001

Note: Data are shown as number (%).
Abbreviations: AS, amygdala sign; CIS, cingulate island sign; OTS, occipital tunnel sign.

3.4 | Radiomic features and machine learning analysis

Based on the SPM-based segmentation process described previously, 39 brain areas were selected for radiomics features extraction and ML classification. Relevant clinical and functional FDG-PET variables were selected by a feature selection algorithm (Boruta) and used to build five ML models, as shown in Table 5.

Regarding the clinical features model, the feature selection algorithm (Boruta) selected the following features: cognitive fluctuation, RBD, and age. According to the random Forest classification analysis, the classification accuracy for these selected clinical features was 63.1%.

Regarding the standard PET features (visual + 3D-SSP) model, the feature selection algorithm (Boruta) selected the following features: occipital hypometabolism, CIS, OTS, anterior cingulate R, precuneus R, precuneus L, parietal superior L, occipital lateral R, and temporal mesial L. According to the random Forest classification analysis, the classification accuracy for these selected FDG-PET features was 84.3%. When this model was run with the DLB signs semi-quantitatively evaluated (e.g., CIS ratio, OTS ratio, AS right, and left ratio), the diagnostic accuracy was lower (73.6% vs 84.3%). Therefore, model 4 all PET features (standard PET features + radiomics features), and model 5 overall features (all PET features + clinical features) were built using visual DLB signs (e.g., occipital hypometabolism, CIS, OTS, and AS).

TABLE 3 Diagnostic performance of FDG-PET hypometabolic pattern (DLB-like pattern vs AD-like pattern), and the DLB hallmark signs (i.e., occipital hypometabolism, cingulate island sign, occipital tunnel sign, and amygdala sign) in the diagnosis of DLB according to final clinical diagnosis (MDT).

	Hypometabolic pattern	Occipital hypometabolism	CIS	OTS	AS
Sensitivity	76.5%	79.4%	64.7%	64.7%	58.8%
Specificity	100%	77.8%	96.3%	96.3%	88.9%
Diagnostic accuracy	86.9%	78.7%	78.7%	78.7%	72.1%
Positive predictive value	100%	81.8%	95.7%	95.7%	87.0%
Negative predictive value	77.1%	75.0%	68.4%	68.4%	63.2%

Note: DLB-like metabolic pattern: hypometabolism in lateral/medial occipital cortex, temporoparietal cortex, and frontal cortex, along with a relative preservation of the mid/posterior cingulate region; AD-like metabolic pattern: hypometabolism in the precuneus/posterior cingulate, parietal cortical territories, and medial and lateral temporal cortex.
Abbreviations: AS, amygdala sign; CIS, cingulate island sign; OTS, occipital tunnel sign.

TABLE 4 Brain areas with a significant difference in mean *Z*-score values at semi-quantitative analysis with 3D-SSP (Cortex ID).

						ROC curve analysis	
Brain areas	MDT diagnosis	*N*	*Z*-score		*p*	Cut-point	AUC
Precuneus R	AD	26	−2.180	(1.076)	0.006	−2.79	0.727
	DLB	28	−3.146	(1.393)			
Parietal superior R	AD	26	−2.129	(1.026)	0.025	−2.81	0.707
	DLB	28	−2.897	(1.380)			
Parietal superior L	AD	26	−1.832	(1.046)	0.045	−3.09	0.678
	DLB	28	−2.636	(1.719)			
Occipital lateral R	AD	26	−1.140	(1.112)	<0.001	−2.12	0.782
	DLB	28	−2.352	(1.368)			
Occipital lateral L	AD	26	−1.401	(1.323)	0.027	−1.76	0.694
	DLB	28	−2.361	(1.739)			
Primary visual R	AD	26	−0.151	(0.993)	0.001	−0.55	0.747
	DLB	28	−1.188	(1.244)			
Primary visual L	AD	26	−0.277	(1.421)	0.017	−1.06	0.712
	DLB	28	−1.199	(1.317)			

Note: Z-score values are shown as means (SD). R: right; L: left; AUC: area under the curve. On the right-hand side of the table, the results of receiver-operating characteristic (ROC) curve analysis with optimal *Z*-score cut-point value, along with AUC for the diagnosis of DLB are reported. Negative FDG-PET scans were excluded.
Abbreviations: AD, Alzheimer's Disease; DLB, Dementia with Lewy Bodies.

According to the feature selection algorithm (Boruta), four PET-derived radiomics features were selected: energy prefrontal medial R, kurtosis parietal superior L, variance fusiform R, and skewness vermis. According to the random Forest classification analysis, the classification accuracy for these selected radiomics features was 73.6%.

Regarding the all PET features (standard PET features + radiomics features) model, the feature selection algorithm (Boruta) selected the following functional features: occipital hypometabolism, OTS, anterior cingulate R, precuneus R, occipital lateral R, kurtosis parietal Sup L, skewness vermis, and variance fusiform R. According to the random Forest classifier, the classification accuracy for these FDG-PET features was 78.9%.

Regarding the overall features (all PET features+ clinical features) model, the feature selection algorithm (Boruta) selected the following features: cognitive fluctuation, RBD, occipital hypometabolism, CIS, OTS, precuneus R, precuneus L, occipital lateral R, kurtosis parietal sup L, skewness vermis, and variance fusiform R. According to the random Forest classification analysis, the classification accuracy was 78.9%.

In Table 6, the classifier's performance evaluated using common statistical metrics on the testing sets of the five different data sets is summarized. Specifically, it includes specificity, sensitivity, precision for AD, precision for DLB, and accuracy in the diagnostic prediction of final clinical diagnosis (MDT). Figure 2 shows the importance of features for the random Forest classifier for the overall features model (ML model 5). Table S2 compared features selected with Boruta according to the participants included in the training set and testing sets.

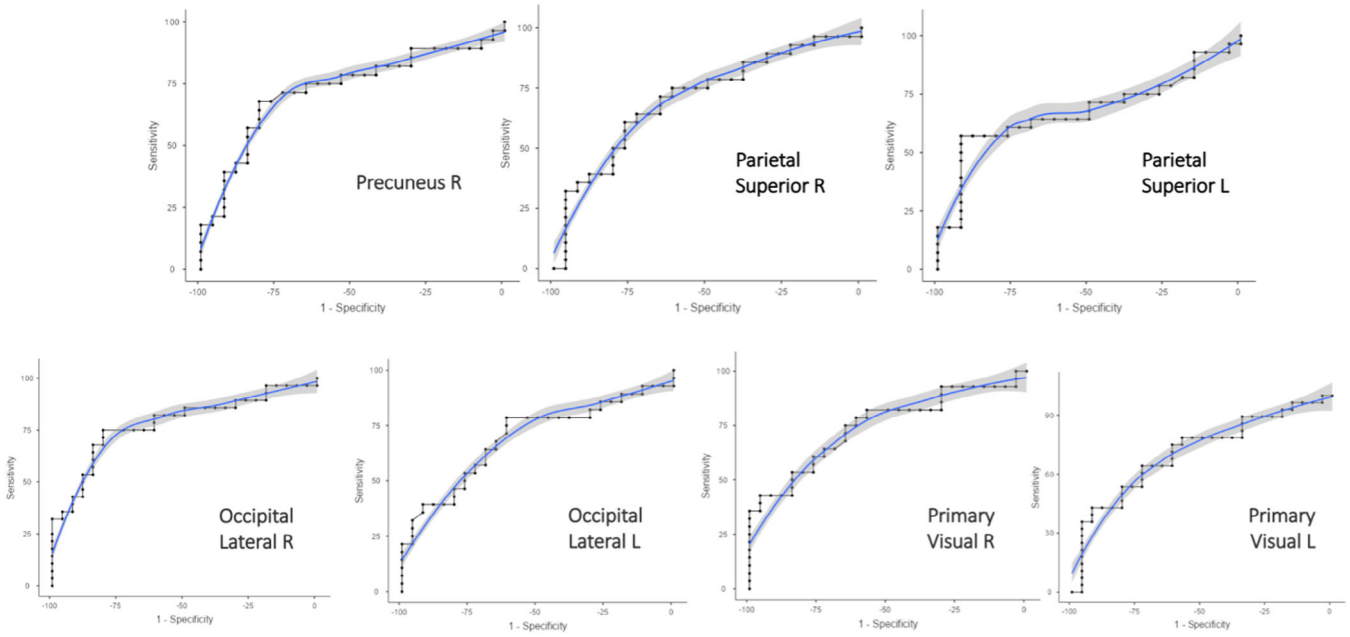

FIGURE 1 Receiver-operating characteristic (ROC) curves of the accuracy of semi-quantitative analysis in the differential diagnosis between dementia with Lewy bodies (DLB) and Alzheimer's disease (AD) in each brain area with a significant difference in *Z*-score from 3-dimensional stereotactic surface projections (3D-SSP) (CortexID).

TABLE 5 Features selected by Boruta algorithm for each of the five machine learning models and corresponding diagnostic accuracy.

Clinical features	Standard PET features (visual + 3D-SSP)	Radiomics features	All PET features	Overall features
Cognitive fluctuation	Occipital hypometabolism	Energy prefrontal medial R	Occipital hypometabolism	Cognitive fluctuation
RBD	CIS	Kurtosis parietal sup L	OTS	RBD
Age	OTS	Variance fusiform R	Anterior cingulate R	Occipital hypometabolism
	Anterior cingulate R	Skewness vermis	Precuneus R	CIS
	Precuneus R		Occipital lateral R	OTS
	Precuneus L		Kurtosis parietal sup L	Precuneus R
	Parietal superior L		Skewness vermis	Precuneus L
	Occipital lateral R		Variance fusiform R	Occipital lateral R
	Temporal mesial L			Kurtosis parietal sup L
				Skewness vermis
				Variance fusiform R
63.1%	**84.3%**	**73.6%**	**78.9%**	**78.9%**

Note: Standard PET features: occipital hypometabolism, cingulate island sign (CIS), occipital sign (OTS), amygdala sign (AS), the *Z*-score values of the brain regions extracted by 3D-SSP (CortexID).
All PET features: the combination of standard PET features (see above) and radiomics features.
Overall features: the combination of all PET features (see above) and clinical features.
Abbreviations: 3-SSP, 3-dimensional stereotactic surface projections; PET, positron emission tomography; RBD, REM sleep behavour disorder.

4 | DISCUSSION

Our study evaluates the diagnostic accuracy of brain FDG PET-CT in the diagnosis of DLB versus AD in a single-center retrospective cohort of patients affected by neurodegenerative dementia. Final clinical diagnosis established by a multidisciplinary meeting after a minimum follow-up of 12 months was used as the ground truth label.[39]

TABLE 6 Diagnostic performance of the five machine learning models, expressed as sensitivity, specificity, precision, and accuracy in the prediction of final clinical diagnosis (MDT).

Machine Learning models	Sensitivity	Specificity	Precision AD	Precision DLB	Accuracy
Clinical features	88%	40%	80%	57%	63.1%
Standard PET features (visual + 3D-SSP)	77%	90%	82%	88%	84.3%
Radiomic features	88%	60%	86%	67%	73.6%
All PET features	77%	80%	80%	78%	78.9%
Overall features	88%	70%	88%	73%	78.9%

Abbreviations: 3-DSSP, 3- dimensional stereotactic surface projections; PET, Positron Emission Tomography.

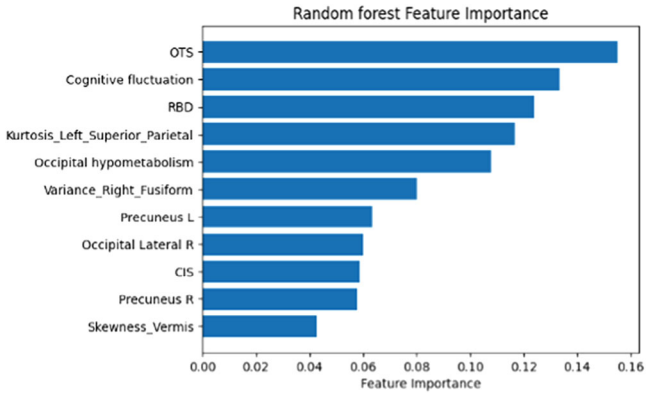

FIGURE 2 Selected features from the random Forest classifier for machine learning model 5 (overall features), describing the relevance of each feature. OTS, Occipital Tunnel Sign; RBD, REM sleep behaviour disorder; CIS, Cingulate Island Sign.

The evaluation of images was the most comprehensive/extensive possible, including the basic and essential visual assessment, a *Z*-score-based semi-quantitative assessment using a well-established software implemented on the workstation (CortexID, 3D-SSP), and extracting radiomics feature with PyRadiomics.

Five ML models were developed to evaluate the diagnostic accuracy of the clinical features of patients (i.e., visual hallucination, cognitive fluctuation, RBD, parkinsonism) and all the data extracted by the analysis of FDG-PET images, including the hallmarks at visual analysis (i.e., occipital hypometabolism, CIS, OTS, AS), the *Z*-score of all the brain areas extracted by CortexID, and radiomics features, matching these overall features in five different combinations.

Our results confirm that FDG-PET is a useful tool in the differential diagnosis of DLB with its most frequent misdiagnosis, AD dementia.

4.1 | Visual analysis

At visual analysis, a typical hypometabolic pattern of DLB/AD was detectable in most patients, with a normal brain FDG-PET scan in slightly more than 10% of the population. This is in line with previous literature, reporting high sensitivity in detecting typical and reliable patterns of brain metabolic dysfunction, also in the early disease phase.[40,41]

When a reduction of cerebral metabolism was evident at visual analysis, FDG-PET showed a high diagnostic accuracy (96.3%) to discriminate DLB from AD according to hypometabolic pattern. However, a relatively high number of false-negative FDG-PET were seen in patients with clinical DLB diagnosis, with consequent slight reduction of sensitivity for this group compared with AD group. Our findings confirm a previous report showing a very high specificity and PPV but a relatively low sensitivity of FDG - PET to diagnose DLB, when evaluated by human expert readers , .[39,42] Indeed, as suggested by Perovnik et al.,[42] lower sensitivity in combination with high specificity shows that expert readers need to recognize clear visual features of the disease and in their study, when they made a final call, they had fewer false-positive readings than their AI model. Of interest, increasing diagnostic accuracy with longer clinical experience was demonstrated.[39]

In our population, all functional FDG-PET signs showed a high and significant association with clinically diagnosed DLB patients.

These data confirm the numerous previously published studies that led to the inclusion of occipital hypometabolism and CIS among the supporting biomarkers in the diagnostic DLB criteria.[6]

The new OTS sign has been described in the literature as a case report,[17] whereas AS was analyzed retrospectively in 49 patients.[18] In this study, the presence of the AS was assessed semi-quantitatively in terms of standardized uptake value, and it was identified in 73.3% DLB subjects compared with 21% AD. In our study, the AS at visual assessment was less frequent in both the DLB group (58.8%) and the AD group (11%). The different FDG-PET image evaluations between the two studies, namely, a semi-quantitative approach in Pillai's manuscript and a qualitative one in our work, could explain the different frequency of AS.

We evaluated the presence of both OTS and AS in a population with DLB and, by comparison, in a group of patients with AD. In our population these signs were associated significantly with DLB compared with AD, with OTS having the best performance in terms of frequency and showing a higher statistical significance than AS.

Furthermore, among all the considered signs, CIS and OTS showed the same results. Indeed, both signs showed the highest

association with DLB, despite being relatively less frequent than occipital hypometabolism. These data should encourage the research collectivity to take into consideration these new visual signs, especially OTS, and to semi-quantitatively validate these signs in larger studies, hopefully having histopathological findings as the gold standard for DLB patients.

In clinical practice, FDG-PET scans are usually assessed visually by nuclear medicine specialists and/or neurologists. When the imaging readers are experts, the diagnostic accuracy of FDG-PET visual assessment is quite high and sufficient to provide a reliable result.[41] However, visual assessment is still prone to errors and inter-rater variability, especially when the readers are not experts and fully automated tools for assessment of FDG-PET are required.[39] Before these tools are integrated in clinical practice, a head-to head comparison with expert's reading is warranted.[42,43]

4.2 | Semi-quantitative analysis

At semi-quantitative analysis, when considering the overall population ($n = 61$) and including PET-negative patients, only one region differed significantly between DLB and AD patients, that is, the left mesial temporal lobe, which had a significant lower *Z*-score in AD patients. This relative preservation in mesial temporal lobe in DLB agrees with the previous findings.[44,45]

On the other hand, when considering only PET-positive patients ($n = 54$), four cortical brain areas showed a significantly lower *Z*-score in DLB compared with AD patients, that is, the right precuneus, bilateral superior parietal, lateral occipital, and primary visual cortices. These results are in line with previous FDG-PET studies showing that DLB patients have significant lower *Z*-scores in the cuneus, precuneus, and parietal lobes, whereas patients with AD have a significant higher occipital/temporal index compared to patients with DLB.[44,46] Moreover, semi-quantitative data seem in accordance with the above qualitative hypometabolic patterns. Nonetheless, quite surprisingly, no significant difference was found in posterior cingulate cortex between DLB (mean *Z*-score -1.7 ± 1.5 on the right and -1.69 ± 1.69 on the left) and AD (mean *Z*-score -1.98 ± 0.98 on the right and -1.96 ± 1.14 on the left). This is in line with the findings of Etminani et al. who showed that a significant hypometabolism in this region is in common in all neurodegenerative dementia forms, including AD, mild cognitive impairment (MCI)-AD, and DLB.[39] Similarly, other authors showed that using an ML-based AD (MAD) designation framework, all patients with dementia showed an AD-like pattern when compared with non-dementia patients[47,48]. Indeed, CortexID *Z*-score measures the deviation of a cortical area in a single subject from the mean of the same area in a cohort of healthy subjects. Therefore, CIS results as a sign a more marked hypometabolism in precuneus compared with posterior cingulate cortex at single patient analysis. Moreover, we cannot exclude a co-pathology in some of our cases.

4.3 | Radiomic features and machine learning models analysis

From the radiomic features extraction, four features resulted significant: energy prefrontal medial R, kurtosis parietal superior L, variance fusiform R, and skewness vermis.

In ML models, in accordance with the literature data, clinical features showed the lowest diagnostic accuracy. PET-derived radiomic features showed better diagnostic accuracy than clinical ones.

The best diagnostic performance of ML model 2 was obtained from the integration of visual hallmark signs of DLB plus *Z*-scores, rather than from a fully semi-quantitative ML model (semi-quantitative DLB hallmark signs plus *Z*-score). Furthermore, this ML model, incorporating the integration of visual DLB signs and semi-quantitative *Z*-score data, has achieved the strongest accuracy in differentiating AD from DLB. This is in line with previous data reporting an increased diagnostic accuracy when visual analysis is powered by semi-quantitative analysis methods.[49,50]

However, differences exist between different semi-quantitative methods, and this gain in accuracy could also be related to different stages of the neurodegenerative pathology.[15,50,51] Therefore, despite the undoubtable potential of a pure quantitative radiomic approach, the real-world usual approach where an expert reader is helped by semi-quantitative methods still has the highest accuracy in making a reliable differential diagnosis between the two pathologies.

When looking at the relative weight of single features in the overall features ML model, OTS shows a higher statistical yield, underlying its potential role in clinical practice. Curiously, OTS and CIS weighted differently despite showing identical frequency and performance on conventional statistical analysis. This is due to the automatized process that aims to reduce redundancy if selected features are linked in the data set.

4.4 | Limitations

A limitation of this study is the possibility of circularity considering that the clinical reference diagnosis was supported and reinforced by different available diagnostic tests, consistent with established diagnostic criteria, including FDG-PET. This could influence the diagnostic accuracy of hypometabolic patterns at visual analysis. However, to reduce this possible bias in the AI analysis, we decided not to include the hypometabolic pattern of FDG-PET in the ML classifier models.

Another limitation of this study is the absence of pathological validation diagnosis.

5 | CONCLUSIONS

In conclusion, our study confirms that differential diagnosis between AD and DLB is challenging when only clinical symptoms and signs are

considered. FDG-PET is a helpful tool to differentiate between these two, sometimes intermingled, clinical entities. Despite the potential for an objective, imaging feature-based radiomic analysis, which could potentially overcome the limitations of FDG-PET reading, especially from less expert readers, real-world usual PET-reading techniques as visual and semi-quantitative analyses still show the highest diagnostic accuracy. Indeed, the qualitative analysis of FDG-PET images, based on the integration of DLB-specific pattern and functional signs, is highly specific for DLB. Moreover, some brain areas are specifically affected and account for significant differences in metabolism at semi-quantitative analysis between the two more common forms of dementia.

Further studies with more consistent samples are needed to verify the diagnostic accuracy of FDG-PET, even in the differential diagnosis with other types of neurodegenerative dementia, possibly having post-mortem pathologic diagnosis as the definitive reference standard.

ACKNOWLEDGMENTS

The work was funded by the Italian Ministry of Health, Grant RF-2018-12366209.

CONFLICT OF INTEREST STATEMENT

All authors report no conflicts of interest.

CONSENT STATEMENT

All subjects signed an informed consent to participate to the study.

REFERENCES

1. Zaccai J, McCracken C, Brayne C. A systematic review of prevalence and incidence studies of dementia with Lewy bodies. *Age Ageing*. 2005;34:561-566.
2. Yousaf T, Dervenoulas G, Valkimadi P-E, Politis M. Neuroimaging in Lewy body dementia. *J Neurol*. 2019;266:1-26.
3. McKeith IG, Burn DJ, Ballard CG, et al. Dementia with Lewy bodies. *Semin Clin Neurpsychiatry*. 2003;8:46-57.
4. Elahi FM, Miller BL. A clinicopathological approach to the diagnosis of dementia. *Nat Rev Neurol*. 2017;13:457-476.
5. Goedert M. Alpha-synuclein and neurodegenerative diseases. *Nat Rev Neurosci*. 2001;2:492-501.
6. McKeith IG, Boeve BF, Dickson DW, et al. Diagnosis and management of dementia with Lewy bodies: fourth consensus report of the DLB consortium. *Neurology*. 2017;89:88-100.
7. Russo M, Carrarini C, Di Iorio A, et al. Accuracy of the clinical diagnosis of dementia with Lewy bodies (DLB) among the Italian Dementia Centers: a study by the Italian DLB study group (DLB-SINdem). *Neurol Sci*. 2022;43:4221-4229.
8. Toledo JB, Cairns NJ, Da X, et al. Clinical and multimodal biomarker correlates of ADNI neuropathological findings. *Acta Neuropathol Commun*. 2013;1:65.
9. Ballard C, Ziabreva I, Perry R, et al. Differences in neuropathologic characteristics across the Lewy body dementia spectrum. *Neurology*. 2006;67:1931-1934.
10. Bonanni L, Thomas A, Tiraboschi P, Perfetti B, Varanese S, Onofrj M. EEG comparisons in early Alzheimer's disease, dementia with Lewy bodies and Parkinson's disease with dementia patients with a 2-year follow-up. *Brain*. 2008;131:690-705.
11. Bousiges O, Blanc F. Biomarkers of dementia with Lewy bodies: differential diagnostic with Alzheimer's disease. *IJMS*. 2022;23:6371.
12. Higuchi M, Tashiro M, Arai H, et al. Glucose hypometabolism and neuropathological correlates in brains of dementia with Lewy bodies. *Exp Neurol*. 2000;162:247-256.
13. Minoshima S, Foster NL, Sima AA, Frey KA, Albin RL, Kuhl DE. Alzheimer's disease versus dementia with Lewy bodies: cerebral metabolic distinction with autopsy confirmation. *Ann Neurol*. 2001;50:358-365.
14. O'Brien JT, Firbank MJ, Davison C, et al. 18F-FDG PET and perfusion SPECT in the diagnosis of Alzheimer and Lewy body dementias. *J Nucl Med*. 2014;55:1959-1965.
15. Caminiti SP, Sala A, Iaccarino L, et al. Brain glucose metabolism in Lewy body dementia: implications for diagnostic criteria. *Alz Res Therapy*. 2019;11:20.
16. Imamura T, Ishii K, Sasaki M, et al. Regional cerebral glucose metabolism in dementia with Lewy bodies and Alzheimer's disease: a comparative study using positron emission tomography. *Neurosci Lett*. 1997;235:49-52.
17. Sawyer DM, Kuo PH. "Occipital Tunnel" Sign on FDG PET for differentiating dementias. *Clin Nucl Med*. 2018;43:e59-61.
18. Pillai JA, Wu G, Tousi B, Larvie M, Léger GC, Leverenz JB. Amygdala sign, a FDG-PET signature of dementia with Lewy bodies. *Parkinsonism Relat Disord*. 2019;64:300-303.
19. Herscovitch P. A pioneering paper that provided a tool for accurate, observer-independent analysis of 18 F-FDG brain scans in neurodegenerative dementias (perspective on "a diagnostic approach in Alzheimer's disease using three-dimensional stereotactic surface projections of fluorine-18-FDG PET". J Nucl Med. 1995;36:1238-1248). *J Nucl Med*. 2020;61:140S-152S.
20. Minoshima S, Frey KA, Koeppe RA, Foster NL, Kuhl DE. A diagnostic approach in Alzheimer's disease using three-dimensional stereotactic surface projections of fluorine-18-FDG PET. *J Nucl Med*. 1995;36:1238-1248.
21. Minoshima S, Frey KA, Foster NL, Kuhl DE. Preserved pontine glucose metabolism in Alzheimer disease: a reference region for functional brain image (PET) analysis. *J Comput Assist Tomogr*. 1995;19:541-547.
22. Minoshima S, Koeppe RA, Frey KA, Kuhl DE. Anatomic standardization: linear scaling and nonlinear warping of functional brain images. *J Nucl Med*. 1994;35:1528-1537.
23. Minoshima S, Mosci K, Cross D, Thientunyakit T. Brain [F-18]FDG PET for clinical dementia workup: differential diagnosis of Alzheimer's disease and other types of dementing disorders. *Semin Nucl Med*. 2021;51:230-240.
24. Nuvoli S, Bianconi F, Rondini M, et al. Differential diagnosis of Alzheimer disease vs. mild cognitive impairment based on left temporal lateral lobe hypomethabolism on 18F-FDG PET/CT and automated classifiers. *Diagnostics*. 2022;12:2425.
25. De Carli F, Nobili F, Pagani M, et al. Accuracy and generalization capability of an automatic method for the detection of typical brain hypometabolism in prodromal Alzheimer disease. *Eur J Nucl Med Mol Imaging*. 2019;46:334-347.
26. Yousefirizi F, Decazes P, Amyar A, Ruan S, Saboury B, Rahmim A. AI-based detection, classification and prediction/prognosis in medical imaging:: towards radiophenomics. *PET Clin*. 2022;17:183-212.
27. Hatt M, Cheze Le Rest C, Antonorsi N, et al. Radiomics in PET/CT: current status and future AI-based evolutions. *Semin Nucl Med*. 2021;51:126-133.
28. Sorbi S, Hort J, Erkinjuntti T, et al. EFNS-ENS guidelines on the diagnosis and management of disorders associated with dementia. *Eur J Neurol*. 2012;19:1159-1179.
29. Guedj E, Varrone A, Boellaard R, et al. EANM procedure guidelines for brain PET imaging using [18F]FDG, version 3. *Eur J Nucl Med Mol Imaging*. 2022;49:632-651.
30. Lim SM, Katsifis A, Villemagne VL, et al. The ^{18} F-FDG PET cingulate island sign and comparison to ^{123} I-β-CIT SPECT for diagnosis of dementia with Lewy bodies. *J Nucl Med*. 2009;50:1638-1645.

31. Van Essen DC, Drury HA, Dickson J, Harwell J, Hanlon D, Anderson CH. An integrated software suite for surface-based analyses of cerebral cortex. *J Am Med Inform Assoc*. 2001;8:443-459.
32. Minoshima S, Frey KA, Koeppe RA, Foster NL, Kuhl DE. A diagnostic approach in Alzheimer's disease using three-dimensional stereotactic surface projections of fluorine-18-FDG PET. 1995;36:1238-1248.
33. Clergue-Duval V, Questel F, Azuar J, et al. Brain 18FDG-PET pattern in patients with alcohol-related cognitive impairment. *Eur J Nucl Med Mol Imaging*. 2020;47:281-291.
34. Tzourio-Mazoyer N, Landeau B, Papathanassiou D, et al. Automated anatomical labeling of activations in SPM using a macroscopic anatomical parcellation of the MNI MRI single-subject brain. *Neuroimage*. 2002;15:273-289.
35. van Griethuysen JJM, Fedorov A, Parmar C, et al. Computational radiomics system to decode the radiographic phenotype. *Cancer Res*. 2017;77:e104-e107.
36. Kursa MB, Rudnicki WR. Feature Selection with the Boruta Package. *J Stat Soft*. 2010;36:1-13. http://www.jstatsoft.org/v36/i11/
37. Breiman L. Random forests. *Mach Learn*. 2001;45:5-32.
38. McKeith I, O'Brien J, Walker Z, et al. Sensitivity and specificity of dopamine transporter imaging with 123I-FP-CIT SPECT in dementia with Lewy bodies: a phase III, multicentre study. *Lancet Neurol*. 2007;6:305-313.
39. Etminani K, Soliman A, Davidsson A, et al. A 3D deep learning model to predict the diagnosis of dementia with Lewy bodies, Alzheimer's disease, and mild cognitive impairment using brain 18F-FDG PET. *Eur J Nucl Med Mol Imaging*. 2022;49:563-584.
40. Perani D, Della Rosa PA, Cerami C, et al. Validation of an optimized SPM procedure for FDG-PET in dementia diagnosis in a clinical setting. *NeuroImage Clin*. 2014;6:445-454.
41. Nobili F, Festari C, Altomare D, et al. Automated assessment of FDG-PET for differential diagnosis in patients with neurodegenerative disorders. *Eur J Nucl Med Mol Imaging*. 2018;45:1557-1566.
42. Perovnik M, Vo A, Nguyen N, et al. Automated differential diagnosis of dementia syndromes using FDG PET and machine learning. *Front Aging Neurosci*. 2022;14:1005731.
43. Nobili F, Arbizu J, Bouwman F, et al. European Association of Nuclear Medicine and European Academy of Neurology recommendations for the use of brain ^{18} F-fluorodeoxyglucose positron emission tomography in neurodegenerative cognitive impairment and dementia: Delphi consensus. *Eur J Neurol*. 2018;25:1201-1217.
44. Iizuka T, Kameyama M. Spatial metabolic profiles to discriminate dementia with Lewy bodies from Alzheimer disease. *J Neurol*. 2020;267:1960-1969.
45. Kantarci K, Boeve BF, Przybelski SA, et al. FDG PET metabolic signatures distinguishing prodromal DLB and prodromal AD. *Neuroimage Clin*. 2021;31:102754.
46. Gjerum L, Frederiksen KS, Henriksen OM, et al. Evaluating 2-[18F]FDG-PET in differential diagnosis of dementia using a data-driven decision model. *NeuroImage Clin*. 2020;27:102267.
47. Lau A, Beheshti I, Modirrousta M, et al. Alzheimer's disease-related metabolic pattern in diverse forms of neurodegenerative diseases. *Diagnostics*. 2021;11:2023.
48. Katako A, Shelton P, Goertzen AL, et al. Machine learning identified an Alzheimer's disease-related FDG-PET pattern which is also expressed in Lewy body dementia and Parkinson's disease dementia. *Sci Rep*. 2018;8:13236.
49. Morbelli S, Chincarini A, Brendel M, et al. Metabolic patterns across core features in dementia with Lewy bodies. *Ann Neurol*. 2019;85:715-725.
50. Massa F, Chincarini A, Bauckneht M, et al. Added value of semiquantitative analysis of brain FDG-PET for the differentiation between MCI-Lewy bodies and MCI due to Alzheimer's disease. *Eur J Nucl Med Mol Imaging*. 2022;49:1263-1274.
51. Brugnolo A, De Carli F, Pagani M, et al. Head-to-head comparison among semi-quantification tools of brain FDG-PET to aid the diagnosis of prodromal Alzheimer's disease. *J Alzheimers Dis*. 2019;68:383-394.

SUPPORTING INFORMATION

Additional supporting information can be found online in the Supporting Information section at the end of this article.

How to cite this article: Mattoli MV, Cocciolillo F, Chiacchiaretta P, et al. Combined 18F-FDG PET-CT markers in dementia with Lewy bodies. *Alzheimer's Dement*. 2023;15:e12515. https://doi.org/10.1002/dad2.12515